New constraints on the future evaporation of the young exoplanets in the V1298 Tau system

A. Maggio,[1] D. Locci,[1] I. Pillitteri,[1] S. Benatti,[1] R. Claudi,[2] S. Desidera,[2] G. Micela,[1] M. Damasso,[3]
A. Sozzetti,[3] and A. Suarez Mascareño[4,5]

[1]*INAF – Osservatorio Astronomico di Palermo, Piazza del Parlamento, 1, I-90134, Palermo, Italy*
[2]*INAF – Osservatorio Astronomico di Padova, Vicolo dell'Osservatorio 5, I-35122, Padova, Italy*
[3]*INAF – Osservatorio Astrofisico di Torino, Via Osservatorio 20, I-10025, Pino Torinese (TO), Italy*
[4]*Instituto de Astrofisica de Canarias, E-38205 La Laguna, Tenerife, Spain*
[5]*Departamento de Astrofisica, Universidad de La Laguna, E-38206 La Laguna, Tenerife, Spain.*

ABSTRACT

Transiting planets at young ages are key targets for improving our understanding of the evolution of exo-atmospheres. We present results of a new X-ray observation of V 1298 Tau with XMM-Newton, aimed to determine more accurately the high-energy irradiation of the four planets orbiting this pre-main-sequence star, and the possible variability due to magnetic activity on short and long time scales. Following the first measurements of planetary masses in the V 1298 Tau system, we revise early guesses of the current escape rates from the planetary atmospheres, employing our updated atmospheric evaporation models to predict the future evolution of the system. Contrary to previous expectations, we find that the two outer Jupiter-sized planets will not be affected by any evaporation on Gyr time scales, and the same occurs for the two smaller inner planets, unless their true masses are lower than $\sim 40\,M_\oplus$. These results confirm that relatively massive planets can reach their final position in the mass-radius diagram very early in their evolutionary history.

1. INTRODUCTION

Planets around young stars deserve special attention, because they allow us to explore the evolutionary history during the first tens of million years after planetary formation. Moreover, the discovery of planetary systems with different architecture with respect to our Solar System has challenged the models of formation and evolution of planets.

One of the first and most puzzling young systems discovered so far with Kepler (K2 mission) is named after the host star V 1298 Tau, a K1 pre-main-sequence dwarf with a near-solar mass, belonging to the Group 29 stellar association (Oh et al. 2017). David et al. (2019) announced a multiple system, including two Neptune-sized planets (dubbed "c" and "d"), one Jovian planet ("b"), and one Saturn-sized planet ("e"), in order of distance from the central star. The three inner planets have well-constrained orbital periods of $\sim 8, 12$, and 24 days, while the outer planet was detected with a single transit event, and hence the orbital period was much more uncertain (40–120 days).

The relatively large planet sizes and rough mass estimates based on simple dynamical arguments suggested as most appealing the scenario of "fluffy" planets still in the contraction phase, due to radiative cooling and/or ongoing photoevaporation processes (David et al. 2019; Poppenhaeger et al. 2021).

In this respect, an assessment of the high-energy environment of the planets is very important, because changes of their masses and sizes on Gyr time scales may depend on the effect of stellar X-rays and UV irradiation onto the primary planetary atmospheres. A wide range of possible evolutionary paths has been recently investigated by Poppenhaeger et al. (2021), but limited by ignorance of the planetary masses and by quite different assumptions on the time evolution of stellar activity.

Intriguing new results from a program of optical spectroscopic observations were presented by Suarez Mascareño et al. (2021) (hereafter SM21). This follow-up campaign provided RV time series sufficiently long to measure the masses of the two outer planets, $M_{\rm p,b} = 203 \pm 60\,M_\oplus$ and $M_{\rm p,e} = 369 \pm 95\,M_\oplus$, and to put

constraints on the masses of the two inner planets, $M_{p,c} < 76.3\,M_\oplus$ and $M_{p,d} < 98.5\,M_\oplus$. An orbital period of $40\pm1\,\mathrm{d}$ was also determined for planet e. All the planetary masses (or upper limits), resulted significantly larger than guessed by David et al. (2019), and even more so with respect to the lower expectations in the "fluffy-planet" scenario, where radii are presumed considerably larger at young ages compared to older planets with the same mass.

In this paper, we discuss first the expected evolutionary path of V 1298 Tau in the H-R diagram (Sect. 2). Next, we present new XMM-Newton observations of the host star (Sect. 3), aimed to determine the possible variability of the high-energy irradiation on short time scales and the spectral hardness of the stellar emission. Then, we revise the most likely evolution of the stellar activity (Sect. 4), and we explore how different models of the X/EUV flux ratio influence the forecasts on the fate of the system, employing a numerical modeling approach developed by Locci et al. (2019) and further refined for the present work (Sect. 5). We discuss the results and draw conclusions in Section 6.

2. STAR AGE AND EVOLUTIONARY PATH

V 1298 Tau is a K1 star with a mass of $1.17\pm0.060\,M_\odot$, a radius of $1.278 \pm 0.070\,R_\odot$, an effective temperature $T_{\rm eff} = 5050\pm100\,\mathrm{K}$, and a bolometric luminosity $L_{\rm bol} = 0.954 \pm 0.040\,L_\odot$ (SM21). It is located at a distance of $108.6 \pm 0.7\,\mathrm{pc}$ toward the Taurus region, and it belongs to the Group 29 stellar association (Oh et al. 2017).

Given the young age of our planet-hosting star, it is important to assess its current position in the theoretical temperature–luminosity diagram, and its evolutionary path up to the age of mature solar-type stars like the Sun. To this aim, we have adopted the PISA evolutionary tracks (Dell'Omodarme et al. 2012). In Figure 1 we show the current position of V 1298 Tau with respect to the tracks for stars of 1.1 $M_\odot$ and 1.2 $M_\odot$. We also show an intermediate interpolated track that yields a mass of $\sim 1.15\,M_\odot$ for V 1298 Tau, in agreement with the value reported by SM21, and an age of $11.9^{+2.0}_{-3.2}\,\mathrm{Myr}$, considering the uncertainties on the effective temperature and bolometric luminosity. This age falls in the range 10–30 Myr reported by SM21 for members of the Group 29 stellar association (Oh et al. 2017), but we note that this range is clearly too large to assess the future evolution of our target in the temperature–luminosity diagram. The position of V 1298 Tau with respect to the PARSEC isochrones (see Fig. 4 in SM21) suggests an age at the younger extreme of this range. In fact, using a Bayesian inference method, SM21 have also constrained
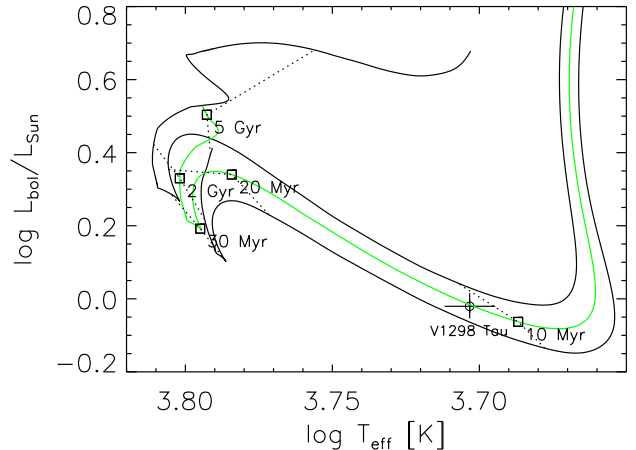

Figure 1. Evolutionary track for V 1298 Tau (in green) in the temperature–luminosity diagram, according to the PISA models (Dell'Omodarme et al. 2012). Adjacent tracks (in black) are for stars of 1.1 $M_\odot$ and 1.2 $M_\odot$. Dotted segments join points at selected ages indicated near the square symbols.

the age of V 1298 Tau to $9\pm2\,\mathrm{Myr}$, which is more in line with our current estimate.

The above analysis indicates that the bolometric luminosity of V 1298 Tau is just above the minimum reached at the end of the Hayashi phase. It will increase by about a factor of two in the next 10 Myr, before landing on the ZAMS as a G-type star at an age of $\sim 30\,\mathrm{Myr}$, and by more than a factor of three until an age of 5 Gyr. This evolution in effective temperature and bolometric luminosity is relevant for assessing the change of the equilibrium temperature of the planets and hence the Jeans escape parameter of their atmospheres (Appendix A).

3. XMM-NEWTON OBSERVATION

The XMM-Newton observation of V 1298 Tau was performed on 2021 February 24 (ObsId 0864340301, PI A. Maggio), with the aim to assess the spectrum and time variability of the host star in X-rays, and hence to characterize the coronal activity level and the dose of high-energy radiation received by its young planets. The exposure time was about 30 ks and the prime instrument was EPIC with FULL FRAME window imaging mode and the MEDIUM filter. Data were obtained with all the CCD-based EPIC cameras and also with the high-resolution RGS spectrometers.

The Observation Data Files were reduced with the Science Analysis System (SAS, ver.18.0.0), following standard procedures. We obtained FITS lists of X-ray events detected with all the EPIC CCD cameras (MOS1, MOS2, and pn) and with the two high-resolution spectrographs (RGS1 and RGS2), calibrated in energy, ar-

Table 1. Best-fit parameters from modeling of the EPIC and RGS spectra of V 1298 Tau.

N_H	T1	EM1	T2	EM2	T3	EM3	χ^2	d.o.f.	f_X	L_X
$10^{20}\,\mathrm{cm}^{-2}$	$10^6\,\mathrm{K}$	$10^{52}\,\mathrm{cm}^{-3}$	$10^6\,\mathrm{K}$	$10^{52}\,\mathrm{cm}^{-3}$	$10^6\,\mathrm{K}$	$10^{52}\,\mathrm{cm}^{-3}$			$10^{-12}\,\mathrm{erg\,s}^{-1}\,\mathrm{cm}^{-2}$	$10^{30}\,\mathrm{erg\,s}^{-1}$
$1.0^{+3.3}_{-1.0}$	$3.0^{+1.4}_{-0.5}$	$2.8^{+3.2}_{-1.3}$	$8.3^{+0.5}_{-1.0}$	$7.1^{+2.6}_{-1.9}$	$16.3^{+2.8}_{-3.1}$	$4.1^{+2.6}_{-1.1}$	3818.08	5719	$1.20^{+0.18}_{-0.11}$	$1.69^{+0.24}_{-0.15}$
1.6 (fixed)	$3.0^{+0.9}_{-0.4}$	$3.3^{+1.3}_{-1.1}$	$8.1^{+0.7}_{-0.7}$	$6.9^{+2.8}_{-1.9}$	$15.1^{+3.6}_{-1.7}$	$4.8^{+1.7}_{-1.8}$	3818.13	5720	$1.24^{+0.02}_{-0.04}$	$1.75^{+0.03}_{-0.05}$

	Mg	Fe	Si	C	O	N	Ne
	Abundances and 90% confidence ranges (solar units; Anders & Grevesse 1989)						
FIP (eV)	7.65	7.90	8.15	11.26	13.62	14.53	21.56
free N_H	0.24	0.16	0.19	0.64	0.24	0.51	0.99
	[0.09, 0.42]	[0.11, 0.21]	[0.09, 0.31]	[< 1.74]	[0.14, 0.35]	[0.05, 1.11]	[0.60, 1.35]
fixed N_H	0.21	0.15	0.19	0.71	0.21	0.45	0.89
	[0.10, 0.36]	[0.11, 0.20]	[0.10, 0.29]	[< 1.71]	[0.15, 0.31]	[0.05, 1.00]	[0.65, 1.23]

NOTE—Unabsorbed X-ray flux and luminosity in the 0.1–10 keV band. Errors are quoted at the 90% confidence level.

rival time, and astrometry with the EVSELECT SAS task. Inspection of the light curve of events detected with energies $> 10\,\mathrm{keV}$, allowed us to identify and filter out a relatively small time interval affected by high background.

We found about 60 detected X-ray sources in the EPIC field of view, including two other bright young stellar objects: one is listed as a candidate YSO in SIMBAD (Gaia DR2 51884824140206720) and the other star is HD 284154, which appears also active and presumably young. The three sources have similar X-ray brightness, but HD 282154 appears redder because its spectrum is softer than the one of V 1298 Tau and the other YSO.

V 1298 Tau is sufficiently isolated to allow the extraction of the source signal from a circular region of $40''$ radii for MOS and pn, and local background from an uncontaminated nearby circular region of similar size. With SAS we also produced the response matrices and effective area files needed for the subsequent spectral analysis. RGS source and background spectra were also extracted adopting the standard results of the SAS pipeline. Source X-ray spectra and light curves are shown in Fig. 2.

For the spectral analysis, performed with XSPEC V 12.10.1f, initially we applied a best-fitting procedure only to the EPIC (MOS1, MOS2, and pn) X-ray spectra. We adopted an optically thin coronal emission model composed by three isothermal components (3T, VAPEC), with the abundances of all elements linked to the iron abundance. Eventually, we added also the RGS1 and RGS2 high-resolution spectra, and allowed up to six el-

ements as free parameters: C, N, O, Ne, Mg, Si, and Fe (Table 1). The source spectrum was also multiplied by a global interstellar absorption component (PHABS). A best fit was achieved with a reduced $\chi^2 = 0.67$ for 5719 d.o.f.

Elemental abundances follow a trend typical of young active stars (Maggio et al. 2007; Scelsi et al. 2007), i.e. elements with low First Ionization Potential (FIP), such as Fe, are systematically underabundant with respect to high-FIP elements, such as Ne, with the notable exception of oxygen. Since coronal Ne traces the actual photospheric abundance more closely than other elements (Maggio et al. 2007), our measurement confirms a near-solar metallicity for V 1298 Tau (SM21).

However, this result should be taken with caution, because the V 1298 Tau coronal abundances are quantified with respect to the solar photospheric abundances (Anders & Grevesse 1989), while stellar abundances for each element should be employed for a proper assessment of any FIP effect (Sanz-Forcada et al. 2004).

Since both the hydrogen column density, N_H, and the C abundance were poorly constrained, we performed a final fit by fixing $N_H = 1.6 \times 10^{20}\,\mathrm{cm}^{-2}$, the value derived from the known B–V color excess, $E(B - V) = 0.024 \pm 0.015$ (David et al. 2019), which implies an extinction $A_V = 0.074 \pm 0.05$ and N_H in the range 6.2×10^{19}–$2.7 \times 10^{20}\,\mathrm{cm}^{-2}$. We checked that this uncertainty implies just a 6% additional systematic error on the measured X-ray flux.

The unabsorbed flux and the luminosity of V 1298 Tau are $f_x = 1.19 \times 10^{-12}\,\mathrm{erg\,s}^{-1}\,\mathrm{cm}^{-2}$ and $L_x =$
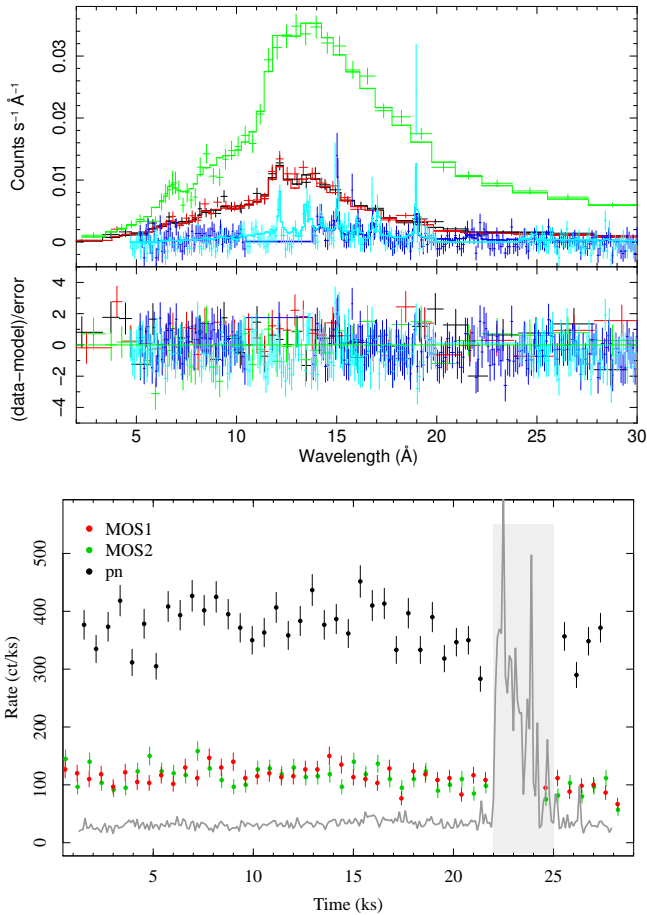
Figure 2. Upper: EPIC and RGS spectra of V 1298 Tau with best-fit model and residuals. Lower: pn and MOS light curves with bin size of 600 s. The gray area marks the region of high background (gray curve), filtered out for the spectral analysis.

$1.68^{+0.03}_{-0.06} \times 10^{30} \, \text{erg s}^{-1}$, respectively, in the band 0.1–2.4 keV. The X-ray to bolometric luminosity ratio resulted $\log L_{\text{x}}/L_{\text{bol}} = -3.35^{+0.01}_{-0.02}$. These values confirm that V 1298 Tau is an X-ray bright young star near the saturated emission regime observed for G-K stars of similar age (Pizzolato et al. 2003; Jackson et al. 2012).

The X-ray light curves of V 1298 Tau (Fig. 2) show time variability on order of 30% with respect to the average rate level during the observation. No large flares were observed.

Poppenhaeger et al. (2021) reported results based on a snapshot X-ray observation ($t_{\text{exp}} \sim 1 \, \text{ks}$) with Chandra, and spectral fitting assuming an isothermal model with fixed solar abundances and negligible interstellar absorption. For comparison, our results show a broad range of coronal plasma components with temperatures ranging from ~ 3 to $\sim 15 \, \text{MK}$, and a pattern of chemical

abundances typical of very active stars (see above). Our total measured X-ray flux is about 25% higher than the flux reported by Poppenhaeger et al. (2021). Considering also the early detection of V 1298 Tau in the ROSAT All Sky Survey, our results imply very little variability of the quiescent X-ray emission on a time scale of about 30 yr, and comparable to the short-term variability that we observed in the time frame of the XMM-Newton observation ($\Delta t \sim 0.35 \, \text{day}$).

4. EVOLUTION OF XUV IRRADIATION

Several formulations were proposed in the past to describe how both the X-ray and the EUV irradiation change in time on Gyr time scales. For the present work, we tested two different descriptions: the simple X-ray luminosity vs. age analytical relation proposed by Penz et al. (2008) (hereafter PM08) for G-type stars, and the most recent semi-empirical modeling by Johnstone et al. (2021) (hereafter J21).

According to PM08, the coronal X-ray luminosity for G-type stars declines with age following a broken power law. It was calibrated considering the X-ray luminosity distributions of stars in the Pleiades and Hyades open clusters, together with field stars and the Sun. The evolutionary path is represented in Fig. 3. The gray area indicates the observed 1σ spread around the median of the X-ray luminosity distribution for the two open clusters. We anchored the starting X-ray luminosity (5–100 Å) of V 1298 Tau to the measured value (Sect. 3), and predicted the future evolution following the same median power-law slopes. In order to predict the EUV luminosity (100–920 Å), we employed the scaling law proposed by Sanz-Forcada et al. (2011) (SF11).

Next, we adopted the description by J21, where the X-ray to bolometric luminosity ratio, $L_{\text{x}}/L_{\text{bol}}$, follows a broken power-law with the Rossby number, i.e. the ratio of the rotation period to the convective turnover time; in this scenario, the evolution of the stellar rotation plays a crucial role, depending on the initial rotation rate at early ages (Ω_0 at $\sim 1 \, \text{Myr}$), the exchange of angular momentum between the stellar core and the convective envelope, the magnetic coupling between the star and the circumstellar disk, and the magnetic braking due to a magnetized stellar wind. All these effects are modeled and calibrated by comparison with observed distributions of stellar rotation periods for stars of different masses and ages. Although this model is clearly more sophisticated than the purely empirical law of PM08, we note that its predictions for a solar-mass star overestimate the observed median X-ray luminosity of the Sun by a factor ~ 5.
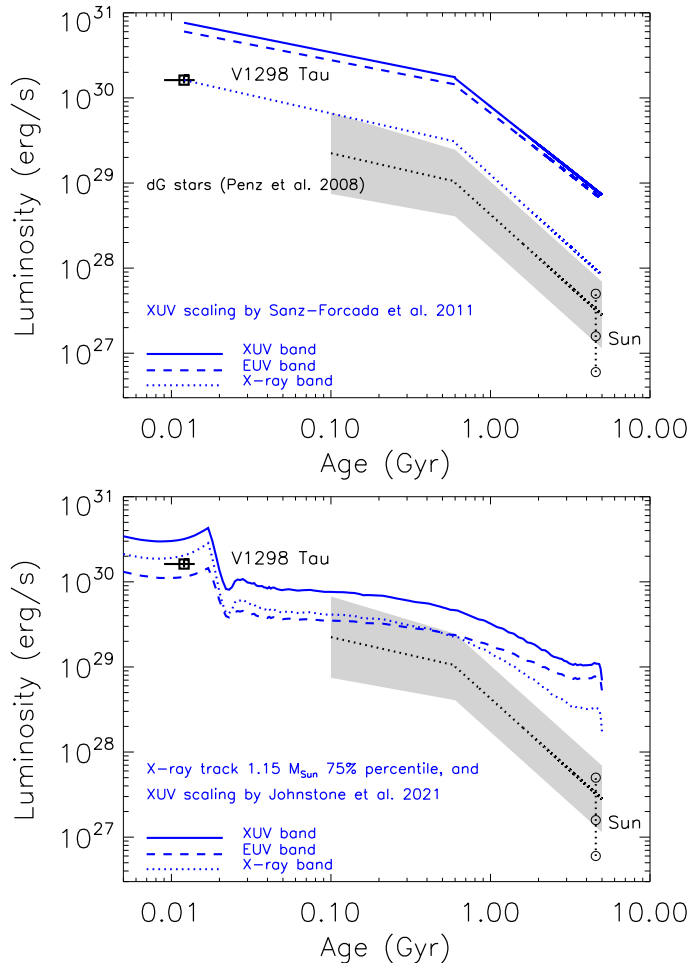
Figure 3. Upper: Time evolution of X-ray, EUV, and total XUV luminosity of V 1298 Tau, according to PM08 and the X-ray/EUV scaling by Sanz-Forcada et al. (2011). The gray area is the original locus for dG stars in PM08. Lower: As above but adopting the evolutionary tracks of J21 for a 1.15 $M_\odot$ star with rotation rate matching the measured value for V 1298 Tau.

We selected as the most appropriate for V 1298 Tau the evolutionary path (Fig. 3) for a 1.15 $M_\odot$ star, with initial rotation rate Ω_0 equal to the current measured value $\Omega = 9.36 \pm 0.16 \, \Omega_\odot$[1], computed from the measured rotation period, $P_{\rm rot} = 2.91 \pm 0.05$ day (SM21). This value of Ω_0 corresponds to the 75% percentile of the observed distribution of rotation rates considered by J21 for stars with similar mass. Our choice is justified self-consistently by the prediction that a star with the mass, age, and rotation rate of V 1298 Tau maintains an almost constant value of Ω from 1 Myr to few hundreds of million of years. In fact, this educated guess of the initial rotation rate identifies an evolutionary track

---

[1] Assuming $\Omega_\odot = 2.67 \times 10^{-6} \, {\rm rad \, s^{-1}}$.

of stellar activity that predicts quite precisely the observed X-ray luminosity of V 1298 Tauand hence defines its most probable future evolution.

Following J21, we have also retrieved the evolutionary path of the EUV luminosity (100–920 Å), predicted on the basis of an empirical mass-independent power-law scaling between the surface EUV and X-ray fluxes, calibrated on a sample of late-type stars observed with the EUVE satellite and solar spectra derived from the TIMED/SEE mission.

Figure 3 clearly shows that the main difference between the PM08+SF11 and J21 descriptions rests on the X-ray/EUV scaling rather than on the X-ray luminosity evolution. In particular, J21 predict a significantly lower EUV luminosity, which becomes larger than the X-ray luminosity only for ages $\gtrsim 600$ Myr. Instead, the SF11 scaling yields higher EUV irradiation at any age, but with a faster decline over time.

To understand the effects of these different descriptions in our photoevaporation modeling, we have also considered a hybrid case in which the X-ray luminosity evolves according to J21 but the EUV luminosity is computed with the SF11 scaling. In summary, we explored three different parameterizations: the analytical formulation by PM08 for the X-ray evolution coupled with the SF11 scaling for the EUV band (PMSF model), the full numerical description by J21 (JoJo model), and a hybrid case with the J21 X-ray evolution coupled with the SF11 scaling (JoSF model).

5. PLANETARY PHOTOEVAPORATION

We investigated the predicted evolution of planetary atmospheres induced by the stellar high-energy radiation, taking into account the updated parameters reported in Sect. 1.

Proceeding similarly as in Georgieva et al. (2021) and in Benatti et al. (2021), we evaluated the mass-loss rate of the planetary atmosphere using the hydrodynamic-based approximation developed by Kubyshkina et al. (2018a) for planetary masses lower than 40 $M_\oplus$, or the energy-limited approximation (Erkaev et al. 2007) for higher values. Then we computed the change in atmospheric mass fraction, planetary mass, and radius, from the present age to 5 Gyr, in steps of 1 Myr, assuming a fixed circular planetary orbit (Appendix A). At any time step, we have employed the Jeans escape parameter (Fossati et al. 2017) to assess if a planet reaches stability against evaporation (Kubyshkina et al. 2018b). A major improvement in our modeling approach with respect to previous applications consisted in taking into account the evolution of the bolometric luminosity (Sect.

Table 2. Modeling results of atmospheric photoevaporation for planets c and d.

					PMSF			JoSF			JoJo		
Case	M_p $(M_\oplus)$	R_p $(R_\oplus)$	M_c $(M_\oplus)$	R_c $(R_\oplus)$	M_f $(M_\oplus)$	R_f $(R_\oplus)$	Δt (Gyr)	M_f $(M_\oplus)$	R_f $(R_\oplus)$	Δt (Gyr)	M_f $(M_\oplus)$	R_f $(R_\oplus)$	Δt (Gyr)
					Planet c								
M_1	38.1		37.1	2.64	37.9	3.42	0.2^a	38.0	3.44	0.22^a	38.1	3.47	0.28^a
M_2	25.4	5.05 ± 0.38	24.6	2.37	24.8	2.71		24.8	2.72		25.1	3.05	
M_3	20.6		20	2.22	20	2.22	1.55^b	20	2.22	2.7^b	20.16	2.7	
M_4	10.3		10	1.84	10	1.84	0.03^b	10	1.84	0.03^b	10	1.84	0.16^b
					Planet d								
M_2	32.6		30.5	2.53	32.1	3.64	1.77^a	32.2	3.68	2^a	32.5	3.8	2.94^a
M_3	21.4	6.30 ± 0.45	20	2.22	20.2	2.79		20.3	2.82		20.6	2.25	
M_4	10.6		10	1.84	10	1.84	0.09^b	10	1.84	0.16^b	10	1.84	1.16^b

NOTES – M_p and R_p are the initial planet mass and radius, M_c and R_c are the assumed core mass and radius, M_f and R_f are the final planet mass and radius at 5 Gyr. [a] Time employed by the planet to become stable against evaporation. [b] Time employed by the planet to lose completely its atmosphere.

2), which factors into the Jeans stability criterion and in determining the size of the gaseous envelope.

We explored different scenarios for the inner planets c and d, having only upper limits on their masses. We considered five possible values: $M_0 = M_{ul}$, i.e. the value of the upper limit, $M_1 = M_{ul}/2$, $M_2 = M_{ul}/3$; instead, M_3 and M_4 were computed assuming a value of 20 and $10\,M_\oplus$ for the core mass, respectively, implying planetary masses between 10% and 30% the current upper limits (Table 2). For comparison, the core mass of Saturn is loosely constrained in the range 5–20 $M_\oplus$ (Helled & Guillot 2013).

As a matter of fact, we found that the most massive outer planets b and e are already stable against evaporation at the initial time. Hence, they are not expected to evolve appreciably. The same occurs for planet c in the case M_0, and for planet d in both the cases M_0 and M_1. This is basically due to a combination of their high density and/or the relatively large distance from the host star.

Instead, in all the other cases, the planets c and d go through a hydrodynamical instability phase, whose intensity and duration depend on their mass. In Figure 4 and in Table 2 we report our results. The latter includes the core mass (M_c) and radius (R_c) for each case, and the planetary mass (M_f) and radius (R_f) at 5 Gyr for each adopted XUV irradiation model. We also report the time (Δt) taken by the planet for losing completely its gaseous envelope or for reaching stability against evaporation, if these conditions occur. In the former case, the cumulative fraction of the atmospheric mass lost reaches 1 (Fig. 4, central panels) and the planetary radius remains equal to the core radius (same figure, right panels). Instead, the stability condition implies a

residual non-null atmospheric mass fraction, but a radius that keeps slowly decreasing due to gravitational shrinking and stellar bolometric luminosity evolution.

We found that stability can be reached only in the case M_1 for planet c, and case M_2 for planet d. For lower masses, the atmospheric mass-loss rate increases, in general, eventually leading to the complete disappearance of the atmosphere. This fate is met by both planets in the M_4 case, independently from the XUV irradiation model adopted. However, different models affect the time required to reach stability or to lose the atmosphere. The case M_3 for planet c is critical in this respect, because complete atmospheric evaporation occurs only if the Sanz-Forcada et al. (2011) X/EUV scaling is considered.

6. DISCUSSION

Our analysis of the high-energy emission level of V 1298 Tau and its short-term variability suggest that this PMS star has a fairly high and steady activity level, typical of coronal sources in the saturated regime (Pizzolato et al. 2003). Comparison of the observed X-ray luminosity with the predictions based on the semi-empirical models of rotation and activity evolution by Johnstone et al. (2021) indicates that our target followed a track with an almost constant rotation rate from 1 Myr to the present age (9–14 Myr). Following this working hypothesis, we can estimate that uncoupling of the star from the circumstellar disk occurred at an age $\tau_d \approx 4.4$ Myr (Tu et al. 2015). This is actually a lower limit to the disk lifetime, i.e. the time available for planets to migrate and accrete rocky material from the disk, and to consequently grow in mass and size.
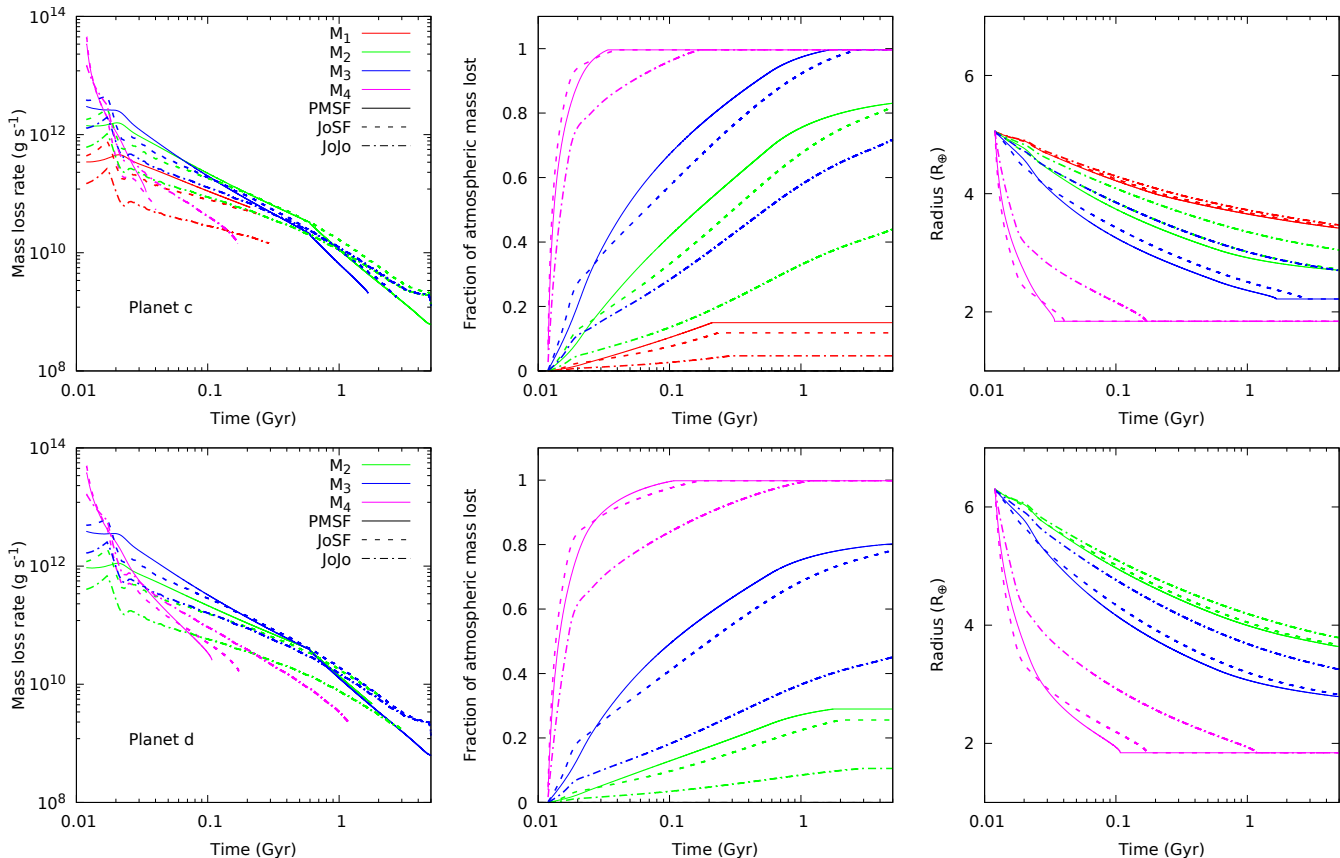
Figure 4. Plots of mass-loss rate, cumulative fraction of atmospheric mass lost, and planetary radius vs. time for planets c and d. In each panel, we use different colors and line styles for each assumed planetary mass and modeling approach.

The relatively large masses for the two outer planets, with respect to their radii, imply quite heavy cores and/or a high metallicity content (SM21), that need to be explained by a detailed modeling of their migration histories. This occurrence implies that they are already stable against photoevaporation, and hence they should not move further from the present position in the mass-radius diagram.

For the inner planets, we conjecture that their characteristics are intermediate between those of Neptune and Saturn. We considered a range of planetary masses 10–$76\,M_\oplus$ for planet c, and 10–$98\,M_\oplus$ for planet d, and estimated atmospheric mass fractions of $\sim 3\%$ for c and 6%–7% for d. We found that they may be affected by photoevaporation only if their true masses are lower than about $40\,M_\oplus$, and they will completely lose their atmospheres if their masses are lower than about $20\,M_\oplus$.

In case of atmospheric photoevaporation, the end state of planetary evolution depends on several factors. The decrease in mass is relatively small with respect to the decrease in radius (by factors 1.5–3), hence the Jeans escape parameter (Eq. A1) tends to increase and hydrodynamical stability could be reached. The oppo-

site trend can be caused by an increase of the bolometric irradiation, leading to an increase of the planetary equilibrium temperature. Moreover, the atmospheric mass-loss rate is larger for planets with lower density, and hence planets with a lower initial mass may completely lose their gaseous envelope before stability is reached.

The mass-loss rate depends on the planetary characteristics that determine its gravitational potential and thermal energy of the atmosphere, but also on the time-variable high-energy irradiation. For planets c and d, our simulations with the models PMSF and JoSF provide similar results for any mass case. Hence, the simple analytical description of the X-ray luminosity evolution vs. age by PM08 results as much effective as the tabulated model by J21 when they are coupled to the same X-EUV scaling by SF11. On the other hand, the JoJo model yields a less vigorous photoevaporation, clearly due to the smaller EUV irradiation predicted at any age. This result shows that the choice of the scaling law for the computation of the total XUV irradiation is relevant in determining the time scale of atmospheric evolution, but the end fate of photoevaporation is identical in most cases.

On the other hand, if mass values near the current upper limits will be assessed for planets c and d with future measurements, their characteristics will not be affected by further atmospheric evolution. We conclude that current measurements are consistent with an evolution of all the four planets much faster than expected so far.

Facilities: XMM (EPIC and RGS)

Software: SAS (Gabriel et al. 2004, www.cosmos.esa.int/web/xmm-newton/sas), XSPEC (Arnaud 1996, heasarc.gsfc.nasa.gov/xanadu/xspec/)

APPENDIX

A. PLANETARY EVOLUTION

According to Fossati et al. (2017), photoevaporation of planetary atmospheres occurs when the Jeans escape parameter

$$\Lambda = \frac{G m_\mathrm{H} M_\mathrm{p}}{k_\mathrm{B} T_\mathrm{eq} R_\mathrm{p}} < 80 \qquad (A1)$$

where G is the gravitational constant, m_H is the hydrogen mass, and k_B is the Boltzman constant, while M_p and R_p are the planet mass and radius, and T_eq is the planet equilibrium temperature, computed as

$$T_\mathrm{eq} = T_\mathrm{eff} \left[f_\mathrm{p} (1 - A_\mathrm{B}) \right]^{1/4} \left(\frac{R_*}{2d} \right)^{1/2} \qquad (A2)$$

where T_eff and R_* are the stellar effective temperature and radius, respectively, A_B is the Bond albedo, d the star–planet distance, and f_p is a parameter that takes into account whether the planet is tidally locked or not. We assumed $A_\mathrm{B} = 0.5$, as for Jupiter, and $f_\mathrm{p} = \frac{2}{3}$, because tidal locking is expected on time scales $\ll 1\,\mathrm{Myr}$, for orbits with negligible eccentricity (Leconte et al. 2010; Ogilvie 2014).

Through T_eff, Λ depends on the stellar bolometric luminosity, and both these parameters enter also in the analytic expression for the atmospheric mass-loss rate derived by Kubyshkina et al. (2018a), which is also a function of the XUV irradiation at the planetary orbital position.

For each initial value of M_p, we calculated the core radius, R_c, through the analytic relation proposed in Benatti et al. (2021) and valid for planets with Earth-like composition. We then computed the radius of the atmospheric envelope as $R_\mathrm{env} = R_\mathrm{p} - R_\mathrm{c}$, and the initial atmospheric mass fraction, $f_\mathrm{atm} = M_\mathrm{env}/M_\mathrm{p}$, by inverting the relation given in Lopez & Fortney (2014). This relation was developed for atmospheres dominated by H–He, and provides R_env as a function of M_p, the bolometric flux received, f_atm, and the age of the system, taking into account also the gravitational shrinking. Furthermore, it allows the choice of solar or enhanced opacity of the atmospheric gas.

In turn, the atmospheric mass fraction allows the computation of the core mass, $M_\mathrm{c} = M_\mathrm{p}(1 - f_\mathrm{atm})$, which we assume constant in time. Alternatively, if the core mass M_c is fixed *a priori*, we can estimate M_p iteratively, given R_env and $f_\mathrm{atm} = 1 - M_\mathrm{c}/M_\mathrm{p}$.

As discussed in SM21, the two outer planets, b and e, show radii that are relatively small with respect to the radii of planets of similar mass, suggesting the presence of a very massive core and/or an extreme enrichment in heavy elements that possibly occurred during their migratory phase. For this reason, we preferred to use for all planets the formulation of Lopez & Fortney (2014) for the case of enhanced atmospheric opacity.

For each time step of the simulation, we updated the planetary mass (and consequently f_atm) in response to

the mass loss, and we employed again the relation by Lopez & Fortney (2014) to compute a new value of R_{env}.

The latter quantity, added to the core radius, provided the updated planetary radius.

REFERENCES

Anders, E., & Grevesse, N. 1989, GeoCoA, 53, 197, doi: 10.1016/0016-7037(89)90286-X

Arnaud, K. A. 1996, in Astronomical Society of the Pacific Conference Series, Vol. 101, Astronomical Data Analysis Software and Systems V, ed. G. H. Jacoby & J. Barnes, 17

Benatti, S., Damasso, M., Borsa, F., et al. 2021, A&A, 650, A66, doi: 10.1051/0004-6361/202140416

David, T. J., Petigura, E. A., Luger, R., et al. 2019, ApJL, 885, L12, doi: 10.3847/2041-8213/ab4c99

Dell'Omodarme, M., Valle, G., Degl'Innocenti, S., & Prada Moroni, P. G. 2012, A&A, 540, A26, doi: 10.1051/0004-6361/201118632

Erkaev, N. V., Kulikov, Y. N., Lammer, H., et al. 2007, A&A, 472, 329, doi: 10.1051/0004-6361:20066929

Fossati, L., Erkaev, N. V., Lammer, H., et al. 2017, A&A, 598, A90, doi: 10.1051/0004-6361/201629716

Gabriel, C., Denby, M., Fyfe, D. J., et al. 2004, in Astronomical Society of the Pacific Conference Series, Vol. 314, Astronomical Data Analysis Software and Systems (ADASS) XIII, ed. F. Ochsenbein, M. G. Allen, & D. Egret, 759

Georgieva, I. Y., Persson, C. M., Barragán, O., et al. 2021, MNRAS, 505, 4684, doi: 10.1093/mnras/stab1464

Helled, R., & Guillot, T. 2013, ApJ, 767, 113, doi: 10.1088/0004-637X/767/2/113

Jackson, A. P., Davis, T. A., & Wheatley, P. J. 2012, MNRAS, 422, 2024, doi: 10.1111/j.1365-2966.2012.20657.x

Johnstone, C. P., Bartel, M., & Güdel, M. 2021, A&A, 649, A96, doi: 10.1051/0004-6361/202038407

Kubyshkina, D., Fossati, L., Erkaev, N. V., et al. 2018a, A&A, 619, A151, doi: 10.1051/0004-6361/201833737

—. 2018b, ApJL, 866, L18, doi: 10.3847/2041-8213/aae586

Leconte, J., Chabrier, G., Baraffe, I., & Levrard, B. 2010, A&A, 516, A64, doi: 10.1051/0004-6361/201014337

Locci, D., Cecchi-Pestellini, C., & Micela, G. 2019, A&A, 624, A101, doi: 10.1051/0004-6361/201834491

Lopez, E. D., & Fortney, J. J. 2014, ApJ, 792, 1, doi: 10.1088/0004-637X/792/1/1

Maggio, A., Flaccomio, E., Favata, F., et al. 2007, ApJ, 660, 1462, doi: 10.1086/513088

Ogilvie, G. I. 2014, ARA&A, 52, 171, doi: 10.1146/annurev-astro-081913-035941

Oh, S., Price-Whelan, A. M., Hogg, D. W., Morton, T. D., & Spergel, D. N. 2017, AJ, 153, 257, doi: 10.3847/1538-3881/aa6ffd

Penz, T., Micela, G., & Lammer, H. 2008, A&A, 477, 309, doi: 10.1051/0004-6361:20078364

Pizzolato, N., Maggio, A., Micela, G., Sciortino, S., & Ventura, P. 2003, A&A, 397, 147, doi: 10.1051/0004-6361:20021560

Poppenhaeger, K., Ketzer, L., & Mallonn, M. 2021, MNRAS, 500, 4560, doi: 10.1093/mnras/staa1462

Sanz-Forcada, J., Favata, F., & Micela, G. 2004, A&A, 416, 281, doi: 10.1051/0004-6361:20034466

Sanz-Forcada, J., Micela, G., Ribas, I., et al. 2011, A&A, 532, A6, doi: 10.1051/0004-6361/201116594

Scelsi, L., Maggio, A., Micela, G., Briggs, K., & Güdel, M. 2007, A&A, 473, 589, doi: 10.1051/0004-6361:20077792

Suarez Mascareño, A., Damasso, M., Lodieu, N., et al. 2021, NatAs, DOI:10.1038/s41550-021-01533-7 doi: 10.1038/s41550-021-01533-7

Tu, L., Johnstone, C. P., Güdel, M., & Lammer, H. 2015, A&A, 577, L3, doi: 10.1051/0004-6361/201526146